communications physics

ARTICLE

https://doi.org/10.1038/s42005-022-00942-y OPEN

Anisotropic MagnetoMemristance

Francesco Caravelli[1]✉, Ezio Iacocca[2], Gia-Wei Chern[3], Cristano Nisoli[1] & Clodoaldo I. L. de Araujo[4]

In the last decade, nanoscale resistive devices with memory have been the subject of intense study because of their possible use in brain-inspired computing. However, operational endurance is one of the limiting factors in the adoption of such technology. For this reason, we discuss the emergence of current-induced memristance in magnetic materials, known for their durability. We show analytically and numerically that a single ferromagnetic layer can possess GHz memristance, due to a combination of two factors: a current-induced transfer of angular momentum (Zhang-Li torque) and the anisotropic magnetoresistance (AMR). We term the resulting effect the anisotropic magneto-memristance (AMM). We connect the AMM to the topology of the magnetization state, within a simple model of a one-dimensional annulus-shaped magnetic layer, confirming the analytical results with micromagnetic simulations for permalloy. Our results open a new path towards the realization of single-layer magnetic memristive devices operating at GHz frequencies.

[1] Theoretical Division (T4), Los Alamos National Laboratory, Los Alamos, NM 87545, USA. [2] Center for Magnetism and Magnetic Materials, University of Colorado, Colorado Springs, CO 80918, USA. [3] Department of Physics, University of Virginia, Charlottesville, VA 22904, USA. [4] Departamento de Fisica, Universidade Federal de Viçosa, Viçosa 36570-900 Minas Gerais, Brazil. ✉email: caravelli@lanl.gov

The development of efficient beyond-von Neumann, bio-inspired, or unconventional computing hinges on the realization of novel devices that can be integrated into traditional circuitry. For this reason, memristive devices are an interesting option. Magnetic materials are promising in this regard because of their integration with CMOS and relatively simple device production. A *memristive device* is 1-port electrical component that satisfies Ohm's law, $V = RI$, and moreover has a dynamical resistance of the form $\frac{dR}{dt} = f(R, I)$[1–3]. An ideal memristor, in which the resistance depends only on the charge $q = \int I(t)dt$ has not been realized yet. Instead, any generic electrical device that exhibits a pinched hysteresis loop in the current–voltage diagram, whether the memory is stored for long or short term, is currently regarded as a memristive device[4].

From an immediate practical perspective, memristive devices are of interest because they can be used as a memory. More broadly, they are studied for their collective behavior and applications in neuromorphic engineering[5]. For instance, the Strukov–Williams memristor, initially identified while studying titanium dioxide[6], can be roughly approximated, far from the resistive boundaries, by the functional form

$$\frac{dR}{dt} = \beta J - \sigma R + \eta, \quad R_{on} \le R(t) \le R_{off}, \tag{1}$$

where J is typically the total current density flowing into the device, while β, σ, and η are constants which need to be determined experimentally. The equation above describes a resistive device whose resistance R is constrained between two values $R_{off} > R > R_{on}$. This is seemingly equivalent to a first-order memristor model with $R(w) = (1 - w)R_{off} + wR_{on}$ and $\frac{dw}{dt} = \alpha w - \beta J$. Note that if $\alpha = 0$, this is an ideal memristor as the internal parameter w can be associated to the charge In general, close to the boundaries R_{off} and R_{on}, Eq. (1) loses its validity. Nonetheless, in a memristive device, the history of its resistance is not uniquely determined by the applied voltage, but depends also on the device internal state.

The use of memory effects in resistive materials has been suggested for a variety of computing applications ranging from logical gates[7–10] to unconventional computing[11–13]; the long term view is that resistive type of memories can perform a variety of tasks ranging from Boolean computation to machine learning[2,3,5]. Within the context of purely electronic memristive devices, their application has focused on hybrid analog-CMOS devices such as crossbar arrays, in which the memristive effect is exploited as memory devices (switches). These are often used in neuromorphic applications via a field-programmable gate array controller, ranging from neural networks to optimization[5]. Such architectures however do not harness the full analog properties of memristive devices, being used as an independent memory unit, with the advantage of being controllable with a single bus. There is a general interest in harnessing the analog power of memristor devices because they exhibit emergent behavior in complex interconnected circuits[5]. For instance, the network of memristors[12,13] can be used for reservoir computing[14] and emergent phenomena such as symmetry breaking and tunneling[15,16].

This work introduces a magnetic memristor which, due to the absence of a tunnel-junction, leads to a smooth response to current, thus making it suitable for analog use. As we discuss in this paper, any soft magnetic material that exhibits anisosotropic magnetoresistance, if the spin transfer torque is non-negligible, should exhibit a memristance. The effect is due to the spin-transfer torque[17], and can access the intrinsic magnetization precession frequencies in the GHz regime[18,19]. Having a GHz memristive device implies that these can operate at frequencies compatible with current CPU speeds, and have the potential to be used symbiotically in neuromorphic-von Neumann computer architectures.

Different types of memristive devices use magnetic materials and rely on magnetoresistance effects. An initial approach was magnetic tunnel junctions[20], relying on current-induced domain wall motion. Moreover, such resistance was shown to depend on differently accessed minor loops, offering a robust multi-level resistive device. More recently, it has been observed that current-induced domain-wall formation in connected Kagomé artificial spin ices[21–23] may give rise to memristive effects.

The use of magnetic materials as a memristive functional element has led to the development of the rapidly growing field of bio-inspired and unconventional computing. Applications and device design include neuromorphic computing with magnetic tunneling junction oscillators[24,25]; reservoir computing via domain walls in arrays of magnetic rings inducing "fading memory"[26], superparamagnetic ensembles[27], and magnetic topological objects[28,29]; and inverse-design or magnonic neural networks[30,31]. In particular, a hysteretic resistive effect based on the giant-magnetoresistance effect has been discussed in[32].

These applications, however, do not rely on a memristive effect as defined in Eq. (1). On this regard, recent evidence for a memristive effect has been presented for exchange-biased bilayers with mHz field sweeps relying on "viscous" dynamics[33] and for a rather exotic spin-glass heterostructure driven by spin-transfer torque in MHz regime[33]. While conforming more closely with Eq. (1), these devices do not achieve GHz memristive effects, thus preventing their integration with current computer architectures.

A naïve expectation is that the intrinsic precessional GHz frequencies of trivial magnetic materials provide a natural environment for memristive effects. Such frequencies can be practically accessed by compensating the magnetic damping with spin-transfer torques[34], e.g., using spin-torque nano-oscillators[24]. It is therefore desirable to fully describe memristive effects originating in a single magnetic material due to current. This is further advantageous from the point of view of scalability and operation speed of fully analog 1-port devices[5].

Here, we analytically demonstrate that a single, trivial ferromagnet exhibits memristive effects at GHz frequencies when an in-plane current both exerts torque via the Zhang-Li mechanism[35] and induces anisotropic magnetoresistance, a combined effect we term *anisotropic magnetomemristance* (AMM). By considering a simple toy model of a 1D ferromagnetic ring, we analytically identify that the memristive effect is enabled by homochiral textures that exhibit a nontrivial topology, akin to spin superfluids[36–38]. This implies that the memristive effect depends on the magnetization state and is, in principle, *reconfigurable*. Physically, the AMM discussed here can be understood as the inertial dynamics of magnetic solitons and its impact on the magnetoresistance of the material. We extend our analysis to micromagnetic simulations where we consider a ferromagnetic annulus with finite thickness. In such a ring, a magnetization state composed of homochiral pairs of domain walls is readily accessible by simple field relaxation, conserving the magnetization's topology, and affording the system with AMM. This allows us to conclude that memristive effects originate from the structural dynamics of the domain walls rather than their current-induced translation.

We summarize here our results. We first develop an analytical framework to study the emergence of AMM in a thin annulus, connecting the current in the device to the voltage drop, and then using the Landau–Lifschitz–Gilbert equation for the dynamics of the magnetization. We then analyze the dynamics of the magnetization in various magnetic states, showing these are stable under certain conditions which we deem "topological". We then analyze numerically, using micromagnetic simulations, a thick annulus, focusing on common permalloy.

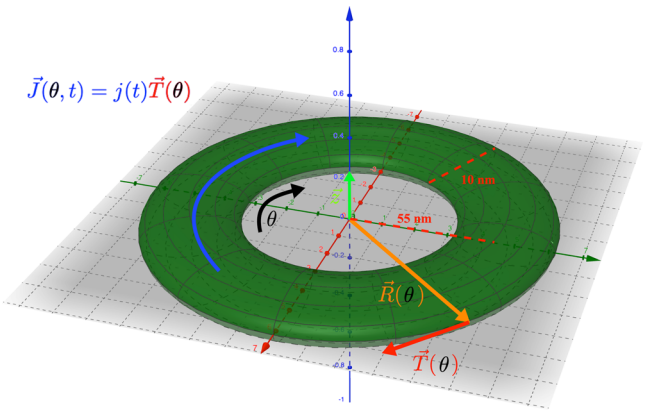

Fig. 1 The geometry of the annulus under study. We consider a nanoscale magnetic device which has the structure of a thick ring, with the dimensions of 10 nm in thickness and 55 nm radius, and vertical dimension of negligible size but finite. The current configuration, $\vec{\boldsymbol{J}}(\theta, t)$ runs along the ring, either clockwise or anticlockwise depending on the sign of $j(t)$. The ring coordinate system is given by $\hat{\boldsymbol{T}}(\theta)$, $\hat{\boldsymbol{R}}(\theta)$ and $\hat{\boldsymbol{z}}$. In the toy model, the thickness of the ring is assumed to be negligible, while in numerical simulations finite size effects are considered.

We expect our results to foster research on analog and reconfigurable memristive devices based on magnetic materials.

Results

Let us now present the main results in the paper. We first develop a theoretical framework to analyze certain magnetic states and formally establish their relationship to resistive and memristive effects. The ideal magnetization states considered in this section allow us to identify the requisites to enable memristance. We will then use this general framework to analyze magnetic states obtained from micromagnetic simulations that take into account nonlocal dipole fields.

Analytical formulation. We begin by considering the first-order correction to the electric field arising in a soft ferromagnet due to AMR[21,22,39]. This correction appears as a combination of current and the magnetization according to[22,39],

$$\vec{\mathbf{E}} = \rho_0 \vec{\mathbf{J}} + \hat{\mathbf{m}}(\rho_{||} - \rho_{\perp})(\hat{\mathbf{m}} \cdot \vec{\mathbf{J}}), \tag{2}$$

where $\rho_{||}$ and $\rho_{\perp}$ are the resistivity parallel and perpendicular to the normalized magnetization vector $\mathbf{m}$, respectively, and $\vec{\mathbf{J}}$ is the current density. We assume $\rho_{||} > \rho_{\perp}$. The first term in Eq. (2) is simply Ohm's law in the continuous medium, while the second term is the first order contribution to the electric field due the AMR effect[39]. In ref. [23], it was shown that it can be recasted as a resistor network with voltage generators in series. Then it is exactly solvable and mapped into an effective memristive effect. While a network analysis is certainly desirable, we focus here on the simple case of a single magnetic element to rigorously derive the memristive effect due to current-induced magnetization dynamics and the magnetization texture.

While the later simulations will be performed for the case of an annulus geometry, the analytical derivations will be done for the case of a ring, e.g., an annulus of negligible thickness. The electrical voltage along a certain path γ is given by $V(t) = \int_{\gamma} \tilde{\mathbf{E}}(\tilde{\mathbf{J}}(t)) \cdot \hat{\mathbf{T}}(\gamma) \mathrm{d}l$, where $\hat{\mathbf{T}}$ is the tangent to the path γ. We consider a ring geometry, whose coordinate system and current physical properties are shown in Fig. 1. Let us thus consider a closed, quasi-one-dimensional path such as a ring of radius r. In this case, γ coincides with the ring itself, so that $\hat{\mathbf{T}}(\theta) = [-\sin\theta, \cos\theta, 0]$ which is a vector oriented clockwise and tangent to the ring at all points, and where $\theta = 0$ corresponds to the positive $\hat{x}$ axis. Assuming that the current circulates tangent to the path, $\mathbf{J}(t, \theta) = j(t)\hat{\mathbf{T}}(\theta)$, then the effective resistivity is given by $\tilde{\rho} = V(t)/(2\pi r j(t))$. Analogously and for later convenience, we also define $\hat{\mathbf{R}}(\theta)$, the in plane vector such that $\hat{\mathbf{R}}(\theta) \cdot \hat{\mathbf{T}}(\theta) = 0$, i.e., parallel to the radius of the ring and directed from the center to the ring point at θ (Fig. 1). In this formulation, we can identify a particular point on the ring via the angular value θ.

Using Eq. (2), we obtain the effective resistivity

$$\tilde{\rho} = \frac{V(t)}{2\pi r j(t)} = \rho_0 + \frac{\Delta\rho}{2\pi} \int_0^{2\pi} \left(\hat{\mathbf{T}}(\theta) \cdot \hat{\mathbf{m}}(\theta)\right)^2 \mathrm{d}\theta. \tag{3}$$

where $\Delta\rho = \rho_{||} - \rho_{\perp}$ and $\hat{\mathbf{m}}(\theta)$ is the normalized magnetization vector expressed at the point θ on the ring. The second term in Eq. (3) depends on the magnetic state and originates from the AMR. From it, we see that the resistivity is constrained by two limiting values, $\rho_{\mathrm{off}} = \rho_0 + \Delta\rho$ and $\rho_{\mathrm{on}} = \rho_0$, the typical resistivity of the material. These two values are typical for the AMR effect. The value ρ_{off} is obtained if $\hat{\mathbf{T}}(\theta) \parallel \hat{\mathbf{m}}(\theta)$, while ρ_{on} if $\hat{\mathbf{T}}(\theta) \perp \hat{\mathbf{m}}(\theta)$. $(\rho_{\mathrm{off}} - \rho_{\mathrm{on}})/\rho_{\mathrm{on}} = \frac{\Delta\rho}{\rho_0}$. Values for $\Delta\rho/\rho_0$ are documented for a variety of materials[39] and it is around 3% for Permalloy.

We are interested in how the effective resistivity of the material changes dynamically. We thus must consider the time evolution of the magnetization vector into Eq. (3). For a ferromagnet subject to an in-plane current, the magnetization dynamics is described by the Landau–Lifshitz–Gilbert (LLG)[40] equation extended with the Zhang-Li torque[35], given by

$$\begin{aligned}\frac{\partial \hat{\mathbf{m}}}{\partial t} = &-\gamma_g \mu_0 \hat{\mathbf{m}} \times \vec{\mathbf{H}}_{\mathrm{eff}} + \alpha \hat{\mathbf{m}} \times \frac{\partial \hat{\mathbf{m}}}{\partial t} - \xi\nu\left(\hat{\mathbf{m}} \times (\tilde{\mathbf{J}}(t) \cdot \nabla)\hat{\mathbf{m}}\right) \\ &- \nu \hat{\mathbf{m}} \times \left(\hat{\mathbf{m}} \times (\tilde{\mathbf{J}}(t) \cdot \nabla)\hat{\mathbf{m}}\right),\end{aligned} \tag{4}$$

where $\nu = \frac{p\mu_0}{eM_S(1+\xi^2)}$, and where we consider the gyromagnetic ratio γ_g, saturation magnetization M_S, the vacuum permeability μ_0, Gilbert damping coefficient α, polarization ratio of the electric current p, electric charge e, and the degree of adiabaticity ξ[35]. The effective field $\vec{\mathbf{H}}_{\mathrm{eff}}$ may include an external magnetic field, magnetocrystalline anisotropy, exchange interaction, and nonlocal dipole fields interaction.

As we show in Supplementary Notes 1 and 2, the combination of both the AMR effect of Eqs. (2) and (4) leads to a time-evolution of the resistivity of the form

$$\frac{\mathrm{d}\tilde{\rho}}{\mathrm{d}t} = \beta(\hat{\mathbf{m}}) j(t) - \eta(\hat{\mathbf{m}}, \vec{\mathbf{H}}_{\mathrm{eff}}), \tag{5a}$$

$$\beta(\hat{\mathbf{m}}) = \beta_a(\hat{\mathbf{m}}) + \beta_{na}(\hat{\mathbf{m}})$$

$$\beta_{na} = -\frac{\xi\nu\Delta\rho}{2\pi r} \int_0^{2\pi} \mathrm{d}\theta \, \frac{\partial \hat{\mathbf{m}}}{\partial \theta} \cdot \left(\hat{\mathbf{T}} \times \hat{\mathbf{m}}\right) t_m \tag{5b}$$

$$\beta_a = \frac{\nu\Delta\rho}{2\pi r} \int_0^{2\pi} t_m(\theta) r_m(\theta) \mathrm{d}\theta \tag{5c}$$

$$\eta(\hat{\mathbf{m}}) = \frac{\Delta\rho}{2\pi} \int_0^{2\pi} \mathrm{d}\theta \left(\gamma_g \mu_0 \vec{\mathbf{H}}_{\mathrm{eff}} - \alpha \frac{\partial \hat{\mathbf{m}}}{\partial t}\right) \cdot \left(\hat{\mathbf{T}} \times \hat{\mathbf{m}}\right) t_m, \tag{5d}$$

$$t_m(\theta) = \hat{\mathbf{T}}(\theta) \cdot \hat{\mathbf{m}}(\theta), \quad r_m(\theta) = \hat{\mathbf{R}}(\theta) \cdot \hat{\mathbf{m}}(\theta), \tag{5e}$$

where $\beta(\hat{\mathbf{m}})$ and $\eta(\hat{\mathbf{m}})$ are functions of the magnetization state in the ring. They indicate how the device reacts to currents and in their absence, respectively. We stress that these equations were derived with the approximation of negligible thickness, e.g., for a ring.

Crucially, Eq. (5a) takes the form of the Strukov-like memristor, described in Eq. (1) in which $\sigma = 0$, while β and η are not constants but depend on the magnetization state and are thus tunable. In particular, the β constant of Eq. (5b) takes the form of a memristive device whose properties depend on the geometry of the ring, such as the radius r, the parameters of the magnetic material, and the magnetization state $\hat{\mathbf{m}}(\theta)$. From the point of view of the theory of memristors, Eq. (5a) represent an infinite-order memristor, i.e., the device depends on a vector field rather then a single parameter (as for instance the doping depth in oxide-based devices).

Equations (5) are the central result of this paper as they rigorously link current-driven magnetization dynamics to memristive effects in magnetic materials subject to AMR effect and Zhang-Li torque. We then call this combined effect the AMM.

A few comments on the equations above are in order. First, the quantities β_{na} and β_a are the magnetization-dependent non-adiabatic and adiabatic coefficients which, if non-zero, induce a memristive effect. Another interesting feature is that the smaller the annulus radius, r, the larger the β_a and β_{na} coefficients are; on the contrary, η does not depend on the annulus radius. This observation implies a crossover between two regimes: a memristive behavior for small radii and a current-independent resistivity change due to the η. In addition, the parameter η contains the balance between the conservative and dissipative terms of the LLG equation. This implies that memristive behavior is primarily due to the magnetization texture present in the material.

In addition to the technical comments above, let us briefly provide here a physical interpretation of the equations. The β term is the term that leads to a memristive effect, as the resistance changes as a function of the current history, and can lead to a pinched hysteresis loop in the current-voltage diagram. Since this term has two components, originating from the adiabatic and non-adiabatic terms in LLG, both contribute to memristance. Because of the vectorial dependence of both these terms, the direction of the magnetization with respect to the plane spanned by the annulus is of key importance. In order for a memristance to be present, the magnetization will have to not lay on the plane, and in particular revolve around the ring, originating from the $\hat{\mathbf{T}}(\theta)\times\hat{\mathbf{m}}$ dependence. In addition to this, the magnetization will also have to be dynamical in a non-trivial manner. For instance, domain walls that can annihilate in the annulus can lead only to a transient memristance, but not a stable one. While these conditions appear to be restrictive, we find that physically achievable magnetic states that cannot be easily removed via spin transfer torque lead to a more stable memristance effect. This is one of the key features of the annulus geometry, which naturally can induce states that are "topological". We will see below that magnetic states that we find to lead to a noticeable memristive states are imperfect, e.g., arising from the interplay of the magnetodynamics of the LLG equation with non-trivial magnetic states.

Naively, one would expect an ideal memristor would be obtained if $\eta = 0$ for any magnetization state and time. However, we must recall that β is not a constant, and thus $\eta = 0$ does not imply that the internal parameter can be directly be associated to the charge. Moreover, $\eta = 0$ is in general unlikely by pure dissipative action on the conservative term since the effective field is nonlocal. However, we will discuss a particular magnetic state in which this is possible. The geometrical terms in the integrand provide other possibilities to nullify η. If $t_m = 0$, which implies a magnetization state perpendicular to the ring's circumference, i.e., pointing radially or fully out-of-plane. The latter state could be easily achieved by a saturating magnetic field applied normal to the plane. However, this condition will also nullify β and the memristive effect would be suppressed. If $\hat{\mathbf{T}}(\theta)\times\hat{\mathbf{m}} = 0$ then the only allowed magnetization state is the ground state, i.e., a magnetization parallel to the ring's circumference. This case also imply that $r_m(\theta) = 0$ and again $\beta = 0$ for all cases. This analysis demonstrates that a magnetic annulus cannot be an ideal memristor.

Magnetization states, resistivity and memristance. We now analyze how certain magnetization patterns could affect the resistance and memristance in this toy model. First, let us note that the resistance depends on $t_m(\theta)$, as $\rho = \rho_0 + \frac{\Delta\rho}{2\pi}\int t_m(\theta)^2 d\theta$ and that there are magnetic states that would lead to no change of resistance and no memristance. We emphasize that the memristive effect is purely due to the interplay between AMR and spin-transfer torque.

Here we focus on the non-adiabatic term, which is larger in real materials. However, an analysis of which states contribute to memristance for the adiabatic term of Eq. (5c) is provided in Supplementary Notes 1, 4, and 5 of the Supplementary Material. In the case of the non-adiabatic term in Eq. (5c), the correction depends on $r_m(\theta)$ and $t_m(\theta)$, which means that the the magnetization must not be perpendicular to both the radius and tangent to the annulus surface at all times.

Thus, a memristive behavior is nullified if the magnetization is everywhere *parallel* to the current or, equivalently, the ring's circumference. A similar fate befalls onto magnetization states where $\partial_\theta\hat{\mathbf{m}} = 0$, i.e., when the device is statically magnetized in a particular direction. This means that memristive effects can only happen as a function of current if the magnetization texture along the annulus is non-trivial.

The typical magnetodynamics scale set by the gyromagnetic ratio and the effective magnetic field is contained in the term $\eta(\theta)$ which produces a change in the device's resistivity in non-equilibrium independent of the current density. In a steady-state, the damping will exactly cancel out any dynamic contribution and $\eta(\theta) = 0$ so that the device will have a finite resistivity. In addition, the effective magnetic field is given by $\overrightarrow{\mathbf{H}}_{\text{eff}} = \overrightarrow{\mathbf{H}}_0 + \lambda\partial^2_{\theta\theta}\hat{\mathbf{m}} - H_k(\hat{\mathbf{m}}\cdot\hat{\mathbf{T}}(\theta))\hat{\mathbf{T}}(\theta)$. Consequently, the main factor determining the memristance is the static magnetization state in the ring.

In addition to trivial magnetization states, it is theoretically possible to have textures in our toy model. Non-trivial magnetization states in rings have been theoretically suggested as means to store energy in the form of angular momentum[38]. Such a state exhibits a smooth, continuous rotation of the magnetization about its perpendicular-to-plane axis and is formally analogous to mass superfluidity or superconductivity[36]. Indeed, a n annulus provides a suitable geometry to realize periodic boundary conditions that, in principle, would stabilize a spin superflow with a quantized number of periods n in the absence of dipolar fields[37].

We now analyze the predicted resistivity and memristance of a variety of possible magnetization states.

Fully magnetized states. Since both η and β depend on $t_m(\theta)$ and $r_m(\theta)$ which are the projection on the tangent and radial vectors of the ring, any out-of-plane or uniformly in-plane magnetization will lead to a pure resistive state. This can be easily achieved, e.g, by an external field saturating the magnetization.

In real materials, if the sample is prepared in a state in which $\mathbf{m}$ has most of its components in the plane, then the effect of an external field $\mathbf{H}_0$ produces only a small correction to the resistivity. We found (see Supplementary Note 3 of the Supplementary Material) that the correction is of the same order of the out-of-plane component of $\mathbf{m}$, implying that the sample is robust to in-plane external field perturbations.

Topological states. As we have seen, certain natural states on the annulus do not support a memristive effect. Let us now attempt at introducing a set of states with full rotations of the magnetization. We introduce a generic magnetization texture of the form $\hat{\mathbf{m}}(\theta) = \big(\sin(\phi)\cos(n\theta), \sin(\phi)\sin(n\theta), \cos(\phi)\big)$, where $\phi(\theta)$ can be an arbitrary function that represents the out-of-plane component of the texture and n quantifies the topology of the state. When $\phi(\theta) = \pi/2$, the magnetization is fully in-plane and the parameter n defines the number of rotations around the ring. For $n = 1$, we recover the ground or vortex state discussed above. For $n \geq 2$, such an equation describes a smooth, coherent rotation of the magnetization known as a spin superflow stemming from its formal analogy to mass superfluidity[36]. In these states, the homochiral phase rotations along θ lead to a net pure spin current which has lead to proposed applications in storage[38] and long-distance spin transport[37,41–45]. These states are interesting because they should be in principle dynamical and non-easily removable via the spin transfer torque. Unfortunately, from Eq. (5b), a spin superflow leads to $\beta(\theta) = 0$. Another state of interest is obtained when $\phi = \omega\theta$, which we call a helical state. Helical states preclude any AMR change, i.e., $\tilde{R} = R_0$ from Eq. (3). Therefore, neither pure spin superflows nor perfect "helical states" produce memristive effects (see Supplementary Note 5 of the Supplementary Material).

This theoretical analysis allows us to state that only magnetic states with both topological and "helical" characters exhibit memristive effects. This implies that non-trivial states must be artificially created in magnetic materials to support memristive effects. Such non-trivial states generally involve one or more pairs of homochiral domain walls that have been discussed in the context of spin superfluids in nanowires[37,41–43] or in nanorings[46,47] as we discuss below.

Magnetic states dominated by shape anisotropy. Here we would like to discuss how the interplay between long-range interactions and topology can lead to non-trivial memristive relevant states. In realistic magnetic materials, often the long-range dipolar interaction is the dominating force, leading to the so-called shape anisotropy. Combined with the exchange interaction which favors parallel spins, there are two degenerate ground states on a magnetic annulus with magnetization $\hat{\mathbf{m}}(\theta) = \pm\hat{\mathbf{T}}(\theta)$. The magnetization is curled around the annulus either clockwise or counterclockwise. Such minimum energy states are also known as the vortex state[48–50]. The vortex state is an example of magnetic state which possesses AMR, but no memristance. In fact, while this magnetic state contributes to the resistivity, it is not hard to see that β_a is zero as $r_m(\theta)$ is zero everywhere; β_{na} is alzo zero as $\hat{\mathbf{T}}(\theta)\times\hat{\mathbf{T}}(\theta) = 0$. Thus, the ground state has no memristance, as it is confirmed below via micromagnetics of extensive rings. We numerically find, however, that these states exhibit a small memristive effect when excited with a strong current. This small effect arises from the periodic modification of the ground state that is not captured with the formalism presented so far. A theoretical analysis of this case is presented in Supplementary Note 4 of the Sspplementary Material.

The magnetic texture that interpolates the two different vortex states with opposite circulation is called the domain wall (DW). Since DWs have to be created and destroyed in pairs on a ring, they are also topological defects on top of the minimum energy state. In fact, each DW can be viewed as a mesoscopic object that carries a net magnetic charges: positive charge for a tail-to-tail DW, and negative charge for head-to-head DW. Metastable states on the annulus can thus be classified according to the number $n_{\mathrm{DW}} = 2, 4, \cdots$ of DWs. Importantly, DWs play a crucial part in the memristive effect of a magnetic annulus by allowing for a non-zero non-adiabatic β_{na} term. Since the magnetization $\hat{\mathbf{m}}(\theta)$ changes from $+\hat{\mathbf{T}}(\theta)$ to $-\hat{\mathbf{T}}(\theta)$ in the vicinity of a DW, thus allowing for a finite gradient $\partial\hat{\mathbf{m}}/\partial\theta$. Moreover, magnetization is forced to deviate from the tangent direction $\pm\hat{\mathbf{T}}(\theta)$, giving rise to a nonzero $\hat{\mathbf{T}}\times\hat{\mathbf{m}}$ as well. As indicated in Eq. (5c), these are the two ingredients for a nonzero β_{na} term. As it will be demonstrated in the next section, the two domain-wall states (2DW) indeed exhibits a significant memristance. Experimentally, these states have been observed in magnetic nanorings[48–50]. Numerically, such a pair of domain walls can be readily stabilized by including nonlocal dipole fields.

Simulations for magnetic annulus. The analytical treatment described above provides a useful guide into the phenomenology, but it is limited to an ideal one-dimensional case. In reality, a finite cross-section of a annulus would produce a non-local dipole field that in turn modifies both the stabilized magnetization states and the dynamics. To account for the non-local dipole contribution, we perform micromagnetic simulations with use of the open-source package MuMax3[51] (details are provided in the "Methods" section and Supplementary Note 6 of the Supplementary Materials).

We simulate a Py annulus with a mean radius of 55 nm, a annulus width of 10 nm, and thickness 10 nm. An analysis of the effects of the dimensions of the annulus is provided in Supplementary Note 7 of the Supplementary Materials. We use standard material parameters $M_s = 790$ kA/m, $A = 10$ pJ/m, and $\alpha = 0.01$. The Zhang-Li torque polarization parameter is set to 0.56 and we also include a small non-adiabatic term $\xi = 0.1$, and for permalloy we have $\rho_0 = 123\ \Omega$ nm.

We consider four initial magnetic configurations. In all cases, we follow the relaxation protocol described in the Methods to quench spurious dynamics. The ground state is the magnetization along the ring, stabilized by shape anisotropy, as shown in Fig. 2a obtained numerically. In-plane and out-of-plane magnetized states are achieved applying an external magnetic field of magnitude 1 T along the x and z directions, respectively. Finally, we consider homochiral domain walls stabilized by initializing the magnetization with a finite number of topological defect, and minimizing the energy. The case of two domain walls is shown in Fig. 2b. The final magnetic state is a localized kink of the form $\hat{\boldsymbol{m}}(\theta) = a(\theta)\hat{\boldsymbol{T}}(\theta) + b(\theta)\hat{\boldsymbol{K}}(\theta)$ where we assume $\hat{\boldsymbol{K}}\cdot\hat{\boldsymbol{T}} = 0$, and thus $|\hat{\boldsymbol{m}}|^2 = a(\theta)^2 + b(\theta)^2 = 1$. We have shown in Supplementary Note 5 of the Supplementary Material that such a magnetic state can have both AMR-induced resistance and memristance. This type of states have been obtained seen both numerically and experimentally in the past[46–49]. These states are topologically distinct from the ground state[52].

We analyze the simulation results by computing the change in voltage and the change in resistivity for each state upon the application of a time-varying current density of magnitude j and frequency f. In the following, we discuss variations in voltage, deviating from the resistive state. These can be studied via $\Delta V = (R - \langle R\rangle)j$, with $\langle R\rangle$ being the time average resistance. We see that if R is constant, then $\Delta V = 0$, which is associated to a pure resistance.

For the ground state, in-plane, and out-of-plane magnetization states, the change in voltage versus the current density in a cycle of frequency $f = 1$ GHz is shown in Fig. 3. For these simulations a rather large current density of 10^{12} A/m^2 was used to discern effects above numerical noise. The I–V curves are shown in Fig. 3a, where we see that a memristance effect is not noticeable at a nV scale. This is consistent with the predictions of the toy model.

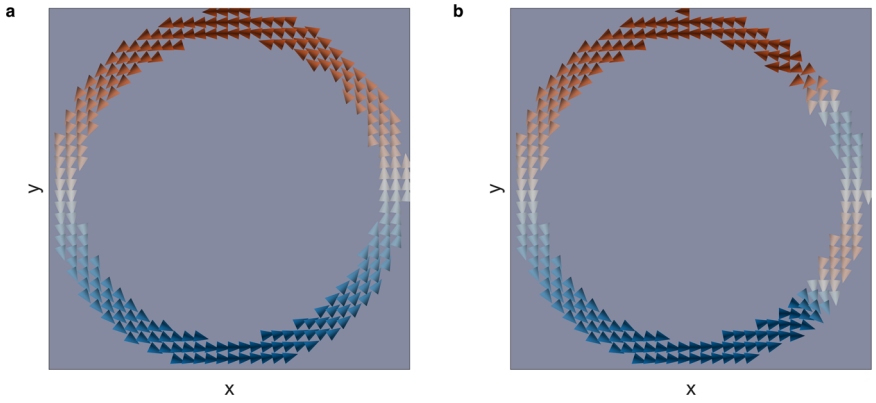

Fig. 2 The magnetic configurations. Stabilized **a** ground state and **b** 2DW (domain wall) state utilizing a tiered energy minimization. The in-plane magnetization component is shown by cones and colored by the m_x value (see Supplementary Movies 1 and 2).

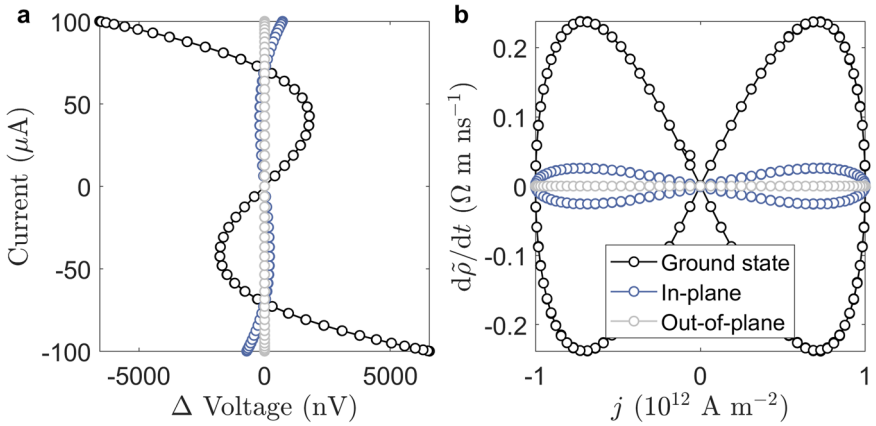

Fig. 3 Hysteresis curves. Change in the resistivity ρ of the ground state (black curve), the in-plane magnetization state (blue) and the out-of-plane magnetic state (light gray). **a** We plot the current–voltage (I–ΔV) diagram of the resistive device as a function of the magnetization. We can see that for currents up to a 100 μA the resistive states do not possess a noticeable hysteresis in the nanovolts. Yet, the anisotropic magnetoresistance (AMR) leads to a nonlinear resistance state. **b** We plot the change in resistivity as a function of the current density j, which is in units of 10^{11} A m^{-2}. From this plot, we can see that the ground state and the in-plane do in fact have a memristance effect, which is however very small. For the out-of-plane state instead, the memristance is zero, as predicted by our model.

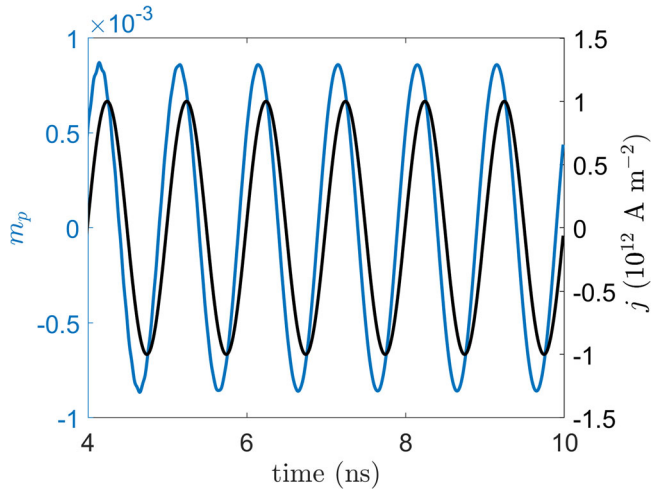

Fig. 4 Averaged magnetization. Spatially averaged magnetization dynamics along the path $T(\theta)$ from micromagnetic simulations of the ground state subject to a microwave current of 1 GHz and amplitude 10^{12} A m^{-2}. The magnetization component m_p is perpendicular to the path $T(\theta)$ is shown by a blue curve and the microwave density current j is shown by a black curve.

However, because the thickness of the annulus gives a small memristance effect that can be seen when looking at $\frac{d\rho}{dt}$. First, $\frac{d\rho}{dt} = 0$ corresponds to pure resistance. That is the case of out-of-plane magnetization. We should expect this property to be true also in real materials with a finite thickness. For the cases of the in-plane and the ground state we note that a small change in resistivity is indeed present, and depends on the current. While a memristance in the ground state and in-plane magnetized state appears to be at odds with the symmetry arguments presented above, we note that the strong current density used in this simulation induces a large enough magnetization dynamics. These dynamics compose a periodic modification that gives rise to a memristive effect, as elaborated in Supplementary Note 4 of the Supplementary Material when discussing the effect of the adiabatic torque component. Figure 4 illustrates these dynamics by plotting the time-evolution of the average magnetization perpendicular to the path $T(\theta)$ (see method for its implementation). The periodicity of the dynamics corresponds to the injection current, demonstrating that this memristive effect originates from time-lagged, current-induced dynamics.

The curves we observe for $\frac{d\rho}{dt}$ are Lissajous curves. Intuitively, this is due to the fact that while the magnetic ground state follows the geometry of the ring, the non-adiabatic coupling leads to a rotation of the magnetization vector. As discussed in

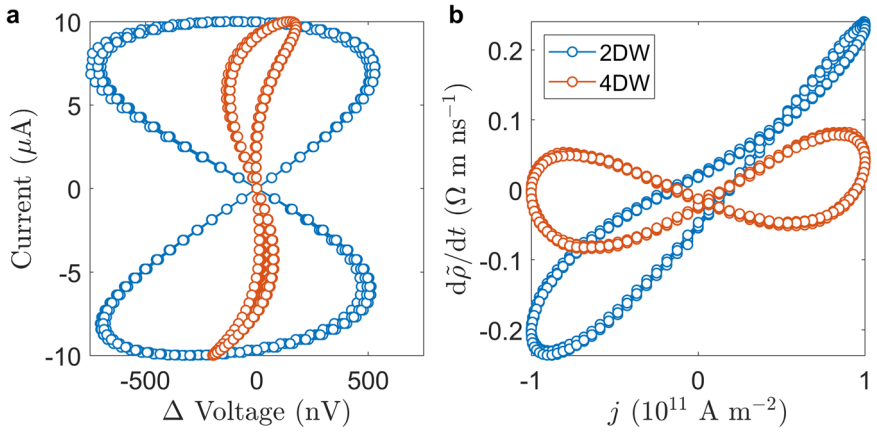

Fig. 5 Hysteresis curves for domain walls (DW). Resistivity of the 2DW and 4DW states. **a** Pinched hysteresis obtained from plotting the device current versus the change in voltage ΔV, in nanovolts. As we can see, the 2DW state has a larger change in voltage, which is of the order of 500 nV. **b** We plot the change in resistivity as a function of the current density, which is in units of 10^{11} A m^{-2}. As we can see, the domain-wall states have a larger memristive effect that the ground state and the in-plane states.

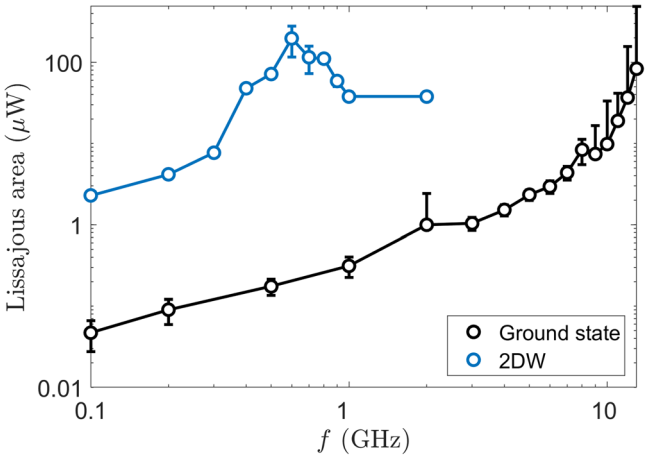

Fig. 6 Size of the memristive effects for domain walls (DW). Area spanned by the curves of the ground state and the 2DW state in Figs. 3 and 5. The area provide an estimate of how large is the change of the resistivity as a function of the frequency of the voltage input per unit of ampere, as in Eq. (5b). The peak in Lissajous area for the 2DW state is at $f = 600$ MHz. The error bars denote standard deviation of the area based on numerical fluctuations and transient effects in the Lissajous' curves.

Supplementary Note 5 of the Supplementary Material, we associate this memristance to an adiabatic effect only accessible at large current densities. We wish to stress that the fact that we observe a non-zero area associated with these curves is indicative of a memristive effect which depends on an internal state. The pinched hysteresis loop in the $\frac{d\rho}{dt}$ vs j diagram implies a zero decay constant η. Indeed, if the change in resistivity was proportional to the current density j, we should expect to see a line in these plots, with a slope given by a constant β parameter. The fact that we see a Lissajous curve means that the parameter β is not constant in time. In particular, the periodicity of β is exactly the one of the driving j.

While for the cases of magnetic in-plane, out-of-plane, and ground states we observe a negligible memristive state, we argue that a non-trivial and measurable effect could be seen for topological magnetic states. In particular, we focus on the domain wall states. The results for two such states with two domain walls (2DW) and 4 domain walls (4DW), and utilizing a current density of 10^{11} A/m^2 are shown in Fig. 5. In particular, in Fig. 5a we plot the current–ΔVoltage diagram, where this time a non-negligible hysteresis can be observed at the nano-volts scale. For the 2DW case, a hysteresis is clearly visible. In Fig. 5b we plot $\frac{d\tilde{\rho}}{dt}$ as a function of the current. We can see that we have a memristance effect with a time varying β constant in both the cases 2DW and 4DW. However, while the curve for the 2DW is pinched, we have a non-pinched hysteresis for the 4DW state, which implies a non-zero (and positive) decay η. This suggests that we can in principle engineer the behavior of the memristor device depending on the annulus internal magnetic state.

A way to estimate and compare how much dependence on the magnetic state we have in the four magnetic states above, is by analyzing the area spanned by the Lissajous curves in $\frac{d\rho}{dt}$ vs. j. In Fig. 6 we plot the estimated area for curves of the ground state and the 2DW state of Figs. 3 and 5 respectively, which are those with the largest hysteresis in the two sets, as a function of the frequency of the input current density. In both cases, the Lissajous' area for the ground state grows with frequency, a further indication that the memristance, in this case, is produced by current-induced dynamics. We do not observe a peak up until 10 GHz. In contrast, the 2DW state peaks at around 600 MHz and exhibits a finite magnitude at 1 GHz, which is larger than the magnetic ground state. The peak at 600 MHz is determined by the most favorable resonance of the coupled 2DW state, determined by the particularities of the energetics. An analytical calculation is beyond the scope of this paper as it necessarily includes the non-local dipole field. However, it is expected that the frequency with maximal Lissajous area will be below ferromagnetic resonance to maintain the spatial localization of domain walls[53]. If this were not the case, then the domain walls would radiate waves and ultimately annihilate (see Supplementary Movie 3). It is worth stressing that while the current densities used for the 2DW state simulations are one order of magnitude smaller than those used for the ground state, the Lissajous area at 600 MHz is approximately two orders of magnitude larger. This demonstrates that the memristance of the 2DW state is primarily due to the magnetization's texture and in good agreement with a memristive device. The key reason why the memristive effect is amplified is that the magnetic kink cannot be easily removed at small currents, which is due to a form of topological protection. In fact, as the current flows, the kink moves due to the Zhang-Li torque, but cannot be easily destroyed. Instead, the domain-wall motion induces a periodic breathing dynamic accompanied by slight modifications in the domain-wall profile. These are shown

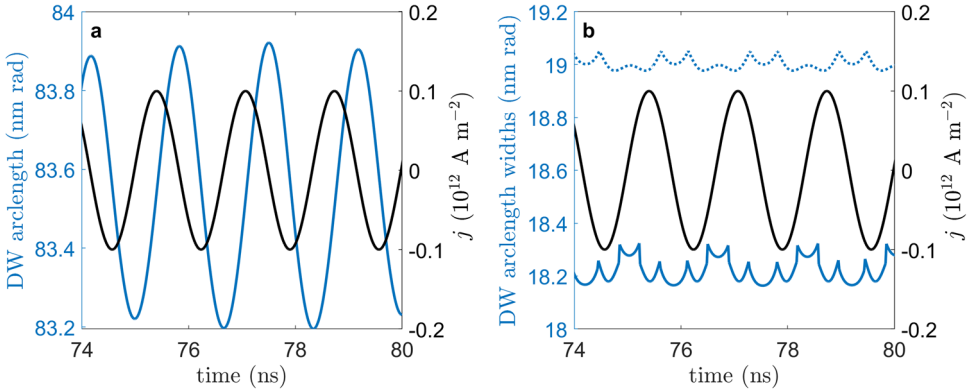

Fig. 7 Averaged magnetization for domain walls (DW). Spatially averaged domain-wall dynamics along the path $T(\theta)$ from micromagnetic simulations of the 2DW state subject to a microwave current density j of 1 GHz and amplitude 10×10^{11} A m^{-2}. The distance between the domain walls is shown to oscillate at the same frequency of the microwave current (black curve) in panel (**a**). The profile of the domain wall is also modified but exhibiting a more complicated pattern in panel (**b**). The solid and dotted lines represent each domain wall width of the 2DW state.

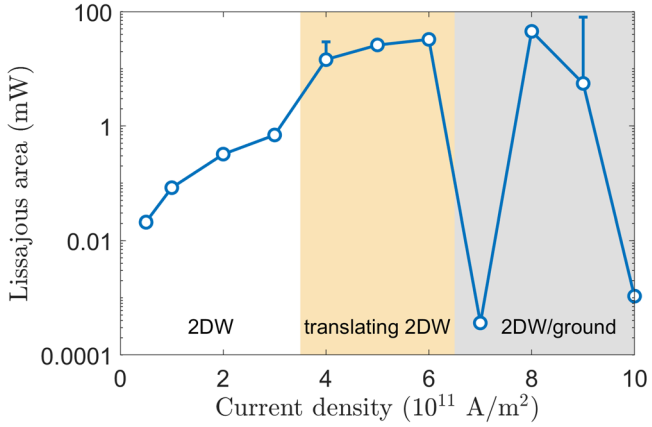

Fig. 8 Fragility of the 2 domain walls (2DW) state. We plot the area of the Lissajous curves as a function of the current density. As we can see, the area of the Lissajous curve depends strongly on the current density, and increases as a function of it. At low densities, the two domain walls are mostly static and the area is small, indicating a negligible memristive effect. At higher densities (yellow area), the domain-walls experience a noticeable distortion accompanied by a small yet finite periodic translation of the domain walls. At much higher current densities (gray area), translation dominates and phase slips can occur, leading to the destruction of the domain-wall pair such that the state of the system stabilizes into its ground state. These cases are evidenced by the low Lissajous areas. The stochastic nature of this regime is due to the cell's large aspect ratio. The error bars denote standard deviation of the area based on numerical fluctuations and transient effects in the Lissajous' curves.

in Fig. 7a, b, respectively, along the path $T(\theta)$. The domain-wall with is estimated by the slope, m, of the profile at its center, $2R/m$, where R is the mean radius of the ring. The microwave current is shown in both cases with a solid black curve. We note that the changes are small but the impact on the voltage is larger due to the details of the configuration in 3D.

Based on the 2DW state, we now explore the current–density dependence on the Lissajous area. The results are presented in Fig. 8. We observe an exponential increase in the area for low current densities that appears to start saturating at 10^{12} A m^{-2}. The sudden jump at large current densities is indicative of a sufficient distortion of the domain walls to untwist the magnetization, i.e., the topological protection is lost and the system relaxes into the ground state. The results of this section provide the intuition that at sufficiently low currents, the magnetic states with a finite rotations about the ring's easy axis are those for which we observe a larger memristive effect. We argue that this observation is associated with the distinct topology of such states when compared to the ground state in the ring. As such, this suggests that in real materials topological protection of the magnetic states is an important ingredient for the observation of a dynamical resistance rooted in the AMR effect. The origin of this protection is indeed due to the fact that we are considering a annulus where these kinks are allowed and not easily annihilated via singularities or phase slips.

A few minor comments are in order. In addition to the analysis above, we have also tested the dependence on the memristance on the annulus radius and the thickness. Our numerical studies (see Supplementary Material) confirms that the thicker the ring, the larger the memristive effect, measured in terms of Lissajous area. Moreover, we have also confirmed that for smaller radii the effect is amplified, in line with the toy model result. However, It is worth mentioning that the Lissajous areas were only slightly affected for larger annulus radii. While more in-depth studies are required, this is encouraging for experiments relying on nanolithography.

Discussion

We have analyzed the memristive effects which occur in realistic magnetic materials due to the interplay between the anisotropic magneto-resistive effect, an electric current via the Zhang-Li coupling, and the magnetodynamics of the material. Our theoretical and numerical results suggest the existence of a memristive effect in trivial ferromagnets by means of the coupled dynamics of domain-walls. This effect is present when the domain-walls exhibit a non-trivial topology that protects the domain walls from annihilating due to current-induced motion. Our study focused on a annulus geometry but the presented results are general as to the physical origin of the effect: the interplay between current-induced dynamics and topology. For the purposes of a rigorous derivation and numerical validation, we have specifically introduced a simple one-dimensional model of a magnetic annulus with an applied voltage and a resulting current, in which the memristive effect due to the Zhang-Li spin-torque interaction between the current and the local magnetization has been derived analytically. This model characterizes explicitly the type of memrisive behavior the device has, and how the non-adiabatic and adiabatic couplings affect the memristive dynamics, e.g., how the resistance changes with the magnetic state.

Our results are based on LLG evolution for the magnetization applied to the Anisotropic-Magnetoresistance effect in continuous

magnetic media. We focused on the study of a common magnetic material such as permalloy, which is readily available. The model explicitly shows that a memristive effect should be present in soft-magnetic material. We predict that for permalloy, it should be measurable at a nano-Volt scale and in the range of 600–1000 MHz.

One of the most striking features of this device is that the behavior of the memristance can be engineered by inducing particular magnetic states. While the effect can be considered small by the standard of typical oxide-devices, we argue that a larger effect should be present in annulii-based lattices, as the change in voltage should accumulate in a coherent fashion. From an experimental perspective, our results are valid for AC currents, implying that for such effect to be observable any DC voltage should be filtered. However, this should be possible using a setup with capacitors or lock-in amplifiers, also given the fact that the effect is in the nV regime. The main experimental challenge might be to stabilize a full rotation of the magnetization in a device that necessarily will depart from a perfect ring, such as a horseshoe geometry, in order to manipulate the magnetization and to inject a microwave current.

From the perspective of the memristive device, engineering the hysteresis is an exciting development. Typically, the hysteresis curves of memristive devices strongly depend on the type of underlying physical properties of the device[4]. While even in numerical experiments we can see that our device is not ideal, we have observed that depending on the magnetic states we can have a non-current dependent memristance decay which is zero.

Crucially, the underlying feature of the amplified memristive effect is a topological protection, enacted by the similar chirality of the domain walls that are only removable by the formation of singularities. The proposed memristor is therefore topological in nature. The possibility of *a posteriori* re-programming the memristor by changing the magnetic properties of the device makes this type of device ideal for a fast neuromorphic Random Access Memory.

This proposal is a departure from previous works on the subject. In fact, other memristive devices based on magnetic states used viscosity to obtain a memristive state, for instance via magnetic pinning[26], domain-wall motion[23], inclusion of magnetic tunnel junctions[24], which induce a slower dynamics. Instead, here we have shown that at the natural timescale (GHz) typical of magnetic dynamics there can be a memristive effect insofar as the stabilized magnetic state is topological.

The present study opens new analyses in this direction. We have analyzed only a handful of magnetic states of a ring. In annulus heterostructures composed of arrays of interconnected rings, the dynamics may interfere additively to increase the total change in the AMR and thus the size of the AMM effect. In other words, we expect that larger structures composed of nanorings will amplify such an effect. Moreover, because we observe an essential topological effect, we expect that such a phenomenon might be observable also in large lattice structures. For instance, by joining rings in a 1d structure, we expect that for large enough currents domain walls can be formed at the junctions. Then, according to our paper, this should correspond to a memristive effect with a threshold dynamics, e.g., for low enough voltages there is no memristance, but at a certain (material dependent) voltage such hysteresis should be expected. This is also the general conclusion of ref. [23], however for a rather simplified toy model. Another possibility is to introduce or combine other magnetoresistive effects. For example, GMR would provide a much larger signal but it will necessarily require coupled magnetic layers. In this case, the coupling between solitons must be carefully studied and related to GMR from the point of view of memristance. It would be interesting to clarify whether a memristive effect would exist at GHz frequencies in this case.

Overall, while this paper does not provide an exhaustive list of magnetic states and geometries that maximize such complex interplay of phenomena, it provides a foundation for the study of this effect. As we have discussed, the memristance effect arises from the combination of dynamical magnetic and non-trivial magnetic states which cannot be easily annihilated due to their topological nature. Based on our analysis, we expect other geometries to satisfy both conditions. A situation of interest is found in 360° domain walls in nanowires. This geometry would provide both a much simpler means to experimentally set a current flow due to its two terminals and an excitation mechanism to produce domain walls at will. Indeed, this geometry has been theoretically studied to date in the context of spin superfluidity[37,41–43], which can be interpreted as a train of homochiral domain-walls. When two domain walls are present, this state is the 1D projection of the 2DW state studied here. Therefore, the same AMM effect is expected. In addition, initial evidence of spin superfluids in antiferromagnets[44,45] also suggests that these effects could be generalized to other materials. Finally, it would be also interesting to explore a two-dimensional version of this effect in lattices of topological objects, such as skyrmion lattices[54,55]. A similar rationale of topology and dynamics suggests that these lattices as a whole could exhibit memristance.

Methods

Sketch of the theoretical derivations. We provide a sketch of the proof of the main formulae provided in the paper, in particular Eqs. (5a)–(5e). The full derivations are provided in Supplementary Note 1 of the Supplementary Material. The key equation which we use as a starting point is the Landau–Lifschitz–Gilbert equation:

$$\begin{aligned}\frac{\partial \hat{\mathbf{m}}}{\partial t} = &-\gamma\mu_0 \hat{\mathbf{m}}\times \vec{\mathbf{H}}_{\text{eff}} + \alpha \hat{\mathbf{m}}\times \frac{\partial \hat{\mathbf{m}}}{\partial t} \\ &- \xi\nu\left(\hat{\mathbf{m}}\times (\vec{\mathbf{J}}(t)\cdot\nabla)\hat{\mathbf{m}}\right) \\ &- \nu\hat{\mathbf{m}}\times \left(\hat{\mathbf{m}}\times (\vec{\mathbf{J}}(t)\cdot\nabla)\hat{\mathbf{m}}\right)\end{aligned} \tag{6}$$

and the AMR correction to the electric field

$$\vec{\mathbf{E}} = \rho_0 \vec{\mathbf{J}} + \hat{\mathbf{m}}(\rho_{||} - \rho_{\perp})(\hat{\mathbf{m}}\cdot\vec{\mathbf{J}}). \tag{7}$$

The voltage drop along a certain path is given by

$$V(t) = \int_{\gamma} \vec{\mathbf{E}}(\vec{\mathbf{J}}(t))\cdot\hat{\mathbf{T}}(\gamma)\mathrm{d}\gamma. \tag{8}$$

Substituting Eq. (7) in Eq. (8) one obtains the voltage in terms of the magnetization.

$$V(t) = \int_{\gamma} \left(\rho_0 \vec{\mathbf{J}} + \hat{\mathbf{m}}(\rho_{||} - \rho_{\perp})(\hat{\mathbf{m}}\cdot\vec{\mathbf{J}})\right)\cdot\hat{\mathbf{T}}(\gamma). \tag{9}$$

If the current is along the annulus then as discussed in the main text, we have

$$\vec{\mathbf{J}}(t) = j(t)\hat{\mathbf{T}}(\theta). \tag{10}$$

Thus, we can define the resistance along a ring, we can define the path γ as $\mathrm{d}\gamma = r\mathrm{d}\theta$, obtaining

$$R(t) = \frac{V(t)}{j(t)} = 2\pi r\rho_0 + r\Delta\rho\int \mathrm{d}\theta\left(\hat{\mathbf{m}}\cdot\hat{\mathbf{T}}(\theta)\right)^2. \tag{11}$$

which is the formula we provided in the main text. Eqs. (5a)–(5e) can now be derived taking a time derivative, and replacing $\frac{\partial \mathbf{m}}{\partial t}$ with the LLG equation.

Numerical simulations. Micromagnetic simulations using MuMax3[51] were performed on a GPU NVIDIA Geforce 940MX. The system is discretized in cells of approximately 1 nm × 1 nm × 10 nm. While the aspect ratio is large, it has been shown in previous works that the numerical effects are negligible for near-uniform states across the thickness[56]. We note that possible instabilities across the thickness would be hidden, but we do not expect such instabilities to exist in uniform or topological states insofar as the magnetization is largely in plane or relatively large in extent[37]. For large current densities, we do observe the compression of the domain wall to an extent where the magnetization is out-of-plane and a phase-slips occur. Such a phase-slip could occur at smaller currents for cubic cells, i.e., via a texture distortion across the thickness. The simulation is set to use a Runge-Kutta 45 stepper and the maximum step time is set to 100th of a period. This is essential to avoid noise for simulations excited by currents of different frequencies.

It is fundamental to stabilize a robust initial condition. The general protocol followed features a "tiered" energy minimization approach to quench spurious dynamics down to numerical accuracy: we first use MuMax's built-in energy minimization function `relax`, then we run for 20 ns with $\alpha = 1$, 30 ns with $\alpha = 0.1$ and 50 ns with $\alpha = 0.01$. The current density is implemented as being parallel to $\mathbf{T}(\theta)$. Such current density is generated in Matlab with and then imported to MuMax3 as a mask whose magnitude is time-dependent.

Dynamic simulations are run for 20 to 100 periods, depending on the frequency of the current. In general, larger frequencies require more time to stabilize into periodic dynamics. This is a consequence of the sudden introduction of current launches spurious spin waves that interact and move the domain wall without resistance because of the lack of material imperfections in the simulations. The resulting time-dependent magnetization dynamics is then processed in MATLAB to obtain the resistivity according to Eq. (3). The change in resistivity $d\tilde{\rho}/dt$ is calculated as the numerical derivative of Eq. (3) while the voltage is simply extracted from Eq. (3) and we consider the average radius of the ring.

The dynamics along the path $T(\theta)$ are extracted from the micromagnetic simulations by transforming space from Cartesian into polar coordinates. A circumference is identified from the midpoint of the ring, within one micromagnetic cell. The resulting data is composed of the in-plane magnetization components as a function of the angle θ. Finally, we implement a rotation matrix to obtain the in-plane magnetization components in polar coordinates, which we identify as m_t (tangential) and m_p (perpendicular).

Data availability

The data that support the findings of this study are available from the corresponding author upon reasonable request.

Received: 29 September 2021; Accepted: 13 June 2022;
Published online: 27 June 2022

References

1. Chua, L. Memristor-the missing circuit element. *IEEE Trans. Circuit Theory* **18**, 507–519 (1971).
2. Jeong, D. S., Kim, K. M., Kim, S., Choi, B. J. & Hwang, C. S. Memristors for energy-efficient new computing paradigms. *Adv. Electron. Mater.* **2**, 1600090 (2016).
3. Serrano-Gotarredona, T., Masquelier, T., Prodromakis, T., Indiveri, G. & Linares-Barranco, B. STDP and STDP variations with memristors for spiking neuromorphic learning systems. *Front. Neurosci.* **7**, 2 (2013).
4. Yang, J. J., Strukov, D. B. & Stewart, D. R. Memristive devices for computing. *Nat. Nanotechnol.* **8**, 13–24 (2012).
5. Caravelli, F. & Carbajal, J. P. Memristors for the curious outsiders. *Technologies* **6**, 118 (2018).
6. Strukov, D. B., Snider, G. S., Stewart, D. R. & Williams, S. The missing memristor found. *Nature* **453**, 80–83 (2008).
7. Wolf, S. A. Spintronics: A spin-based electronics vision for the future. *Science* **294**, 1488–1495 (2001).
8. Ney, A., Pampuch, C., Koch, R. & Ploog, K. H. Programmable computing with a single magnetoresistive element. *Nature* **425**, 485–487 (2003).
9. Patra, M. & Maiti, S. K. All-spin logic operations: Memory device and reconfigurable computing. *EPL (Europhys. Lett.)* **121**, 38004 (2018).
10. Zhang, Y. et al. Spintronics for low-power computing. In *Design, Automation & Test in Europe Conference & Exhibition (DATE), 2014* (IEEE Conference Publications, 2014).
11. Traversa, F. L., Ramella, C., Bonani, F. & Di Ventra, M. Memcomputing NP-complete problems in polynomial time using polynomial resources and collective states. *Sci. Adv.* **1**, e1500031 (2015).
12. Caravelli, F., Traversa, F. L. & Di Ventra, M. Complex dynamics of memristive circuits: Analytical results and universal slow relaxation. *Phys. Rev. E* **95**, 022140 (2017).
13. Caravelli, F. Asymptotic behavior of memristive circuits. *Entropy* **21**, 789 (2019).
14. Du, C. et al. Reservoir computing using dynamic memristors for temporal information processing. *Nat. Commun.* **8**, 2204 (2017).
15. Hochstetter, J. et al. Avalanches and edge-of-chaos learning in neuromorphic nanowire networks. *Nat. Commun.* **12**, 4008 (2021).
16. Caravelli, F., Sheldon, F. C. & Traversa, F. L. Global minimization via classical tunneling assisted by collective force field formation. *Sci. Adv.* **7**, https://doi.org/10.1126/sciadv.abh1542 (2021).
17. Beach, G., Tsoi, M. & Erskine, J. Current-induced domain wall motion. *J. Magn. Magn. Mater.* **320**, 1272–1281 (2008).
18. Silva, T. J. & Rippard, W. H. Developments in nano-oscillators based upon spin-transfer point-contact devices. *J. Magn. Magn. Mater.* **320**, 1260–1271 (2008).
19. Bonetti, S., Muduli, P., Mancoff, F. & Åkerman, J. Spin torque oscillator frequency versus magnetic field angle: The prospect of operation beyond 65 GHz. *Appl. Phys. Lett.* **94**, 102507 (2009).
20. Lequeux, S. et al. A magnetic synapse: multilevel spin-torque memristor with perpendicular anisotropy. *Sci. Rep.* **6**, 31510 (2016).
21. Le, B. L. et al. Understanding magnetotransport signatures in networks of connected permalloy nanowires. *Phys. Rev. B* **95**, 060405 (2017).
22. Chern, G.-W. Magnetotransport in artificial kagome spin ice. *Phys. Rev. Appl.* **8**, 064006 (2017).
23. Caravelli, F., Chern, G.-W. & Nisoli, C. Artificial spin ice phase-change memory resistors. *New J. Phys.* **24**, 023020 (2022).
24. Locatelli, N., Cros, V. & Grollier, J. Spin-torque building blocks. *Nat. Mater.* **13**, 11–20 (2013).
25. Grollier, J., Querlioz, D. & Stiles, M. D. Spintronic nanodevices for bioinspired computing. *Proc. IEEE* **104**, 2024–2039 (2016).
26. Dawidek, R. W. et al. Dynamically driven emergence in a nanomagnetic system. *Adv. Funct. Mater.* **31**, 2008389 (2021).
27. Welbourne, A. et al. Voltage-controlled superparamagnetic ensembles for low-power reservoir computing. *Appl. Phys. Lett.* **118**, 202402 (2021).
28. Prychynenko, D. et al. Magnetic skyrmion as a nonlinear resistive element: A potential building block for reservoir computing. *Phys. Rev. Appl.* **9**, 014034 (2018).
29. Zou, J., Zhang, S. & Tserkovnyak, Y. Topological transport of deconfined hedgehogs in magnets. *Phys. Rev. Lett.* **125**, 267201 (2020).
30. Wang, Q., Chumak, A. V. & Pirro, P. Inverse-design magnonic devices. *Nat. Commun.* **12**, 2326 (2021).
31. Papp, A., Porod, W. & Csaba, G. Nanoscale neural network using non-linear spin-wave interference. *Nat. Commun.* **12**, 6422 (2021).
32. Munchenberger, J., Reiss, G. & Thomas, A. A memristor based on current-induced domain-wall motion in a nanostructured giant magnetoresistance device. *J. Appl. Phys.* **111**, 07D303 (2012).
33. Chen, G., Ivanov, S. & Urazhdin, S. Nearly ideal memristive functionality based on viscous magnetization dynamics. *Appl. Phys. Lett.* **117** 103501-1–103501-5 (2020).
34. Ralph, D. C. & Stiles, M. D. Spin transfer torques. *J. Magn. Magn. Mater.* **320**, 1190–1216 (2008).
35. Zhang, S. & Li, Z. Roles of nonequilibrium conduction electrons on the magnetization dynamics of ferromagnets. *Phys. Rev. Lett.* **93**, 127204 (2004).
36. König, J., Bønsager, M. C. & MacDonald, A. H. Dissipationless spin transport in thin film ferromagnets. *Phys. Rev. Lett.* **87**, 187202 (2001).
37. Iacocca, E., Silva, T. J. & Hoefer, M. A. Breaking of Galilean invariance in the hydrodynamic formulation of ferromagnetic thin films. *Phys. Rev. Lett.* **118**, 017203 (2017).
38. Tserkovnyak, Y. & Xiao, J. Energy storage via topological spin textures. *Phys. Rev. Lett.* **121**, 127701 (2018).
39. McGuire, T. & Potter, R. Anisotropic magnetoresistance in ferromagnetic 3d alloys. *IEEE Trans. Magn.* **11**, 1018–1038 (1975).
40. Gilbert, T. Classics in magnetics a phenomenological theory of damping in ferromagnetic materials. *IEEE Trans. Magn.* **40**, 3443–3449 (2004).
41. Sonin, E. B. Spin currents and spin superfluidity. *Adv. Phys.* **59**, 181–255 (2010).
42. Takei, S. & Tserkovnyak, Y. Superfluid spin transport through easy-plane ferromagnetic insulators. *Phys. Rev. Lett.* **112**, 227201 (2014).
43. Iacocca, E. & Hoefer, M. A. Hydrodynamic description of long-distance spin transport through noncollinear magnetization states: Role of dispersion, nonlinearity, and damping. *Phys. Rev. B* **99**, 184402 (2019).
44. Yuan, W. et al. Experimental signatures of spin superfluid ground state in canted antiferromagnet cr_2o_3 via nonlocal spin transport. *Sci. Adv.* **4**, eaat1098 (2018).
45. Stepanov, P. et al. Long-distance spin transport through a graphene quantum hall antiferromagnet. *Nat. Phys.* **14**, 907 (2018).
46. Tchernyshyov, O. & Chern, G.-W. Fractional vortices and composite domain walls in flat nanomagnets. *Phys. Rev. Lett.* **95**, 197204 (2005).
47. Haraa, M., Shibata, J., Kimura, T. & Otani, Y. Detection of magnetic state in a nanoscale ferromagnetic ring by using ballistic semiconductor two-dimensional electron gas. *Appl. Phys. Lett.* **88**, 082501 (2006).
48. Singh, K. D., Krotkov, R. & Tuominen, M. T. Magnetic transitions in ultra-small nanoscopic magnetic rings: Theory and experiments. *Phys. Rev. B* **79**, 184409 (2009).
49. Zhu, F. Q. et al. Magnetic bistability and controllable reversal of asymmetric ferromagnetic nanorings. *Phys. Rev. Lett.* **96**, 027205 (2006).
50. Liu, H. et al. Magnetic configurations and state diagram of nanoring magnetic tunnel junctions. *Phys. Rev. Appl.* **10**, 054013 (2018).
51. Vansteenkiste, A. et al. The design and verification of mumax3. *AIP Adv.* **4**, 107133 (2014).

52. Braun, H.-B. Topological effects in nanomagnetism: From superparamagnetism to chiral quantum solitons. *Adv. Phys.* **61**, 1–116 (2012).
53. Kosevich, A., Ivanov, B. & Kovalev, A. Magnetic solitons. *Phys. Rep.* **194**, 117–238 (1990).
54. Mühlbauer, S. et al. Skyrmion lattice in a chiral magnet. *Science* **323**, 915–919 (2009).
55. Montoya, S. A. et al. Tailoring magnetic energies to form dipole skyrmions and skyrmion lattices. *Phys. Rev. B* **95**, 024415 (2017).
56. Iacocca, E., Gliga, S. & Heinonen, O. G. Tailoring spin-wave channels in a reconfigurable artificial spin ice. *Phys. Rev. Appl.* **13**, 044047 (2020).

Acknowledgements

The work of F.C. and C.N. was carried out under the auspices of the US Department of Energy through the Los Alamos National Laboratory, operated by Triad National SecurityLLC (Contract No. 892333218NCA000001). C.N. was funded by DOE-LDRD grant 2017014ER. F.C. was also financed via DOE-LDRD grants PRD20170660 and PRD20190195. C.I.L.A. was funded by CNPq 432029/2018-1, FAPEMIG, Coordenação de Aperfeiçoamento de Pessoal de Nível Superior (CAPES) - Finance Code 001 and Newton Fund NAF-R2-192040.

Author contributions

C.I.L.A. and E.I. performed the numerical simulations and F.C. developed and worked on the theoretical model. F.C., C.N., C.I.L.A., E.I., and G.W.C. contributed to the discussions on analytical and numerical results, as well as writing the paper. F.C. and E.I. contributed equally to this work.

Competing interests

The authors declare no competing interests.

Additional information

Supplementary information The online version contains supplementary material available at https://doi.org/10.1038/s42005-022-00942-y.

Correspondence and requests for materials should be addressed to Francesco Caravelli.

Peer review information *Communications Physics* thanks Rachid Sbiaa, Dhritiman Bhattacharya, and the other, anonymous, reviewer(s) for their contribution to the peer review of this work.

Reprints and permission information is available at http://www.nature.com/reprints

Publisher's note Springer Nature remains neutral with regard to jurisdictional claims in published maps and institutional affiliations.